



## Abstract

Using the Community Climate System Model version 3 (CCSM3) including a dynamic global vegetation model a set of 13 interglacial time slice experiments was carried out to study global climate variability between and within the Quaternary interglaciations of Marine Isotope Stages (MIS) 1, 5, 11, 13, and 15. The different effects of obliquity, precession and greenhouse gas forcing on global surface temperature and precipitation fields are illuminated. Several similarities with previous idealized orbital-forcing experiments can be identified. In particular, a significant role of meridional insolation-gradient forcing by obliquity variations in forcing the West African monsoon is found. The sensitivity of the West African monsoon to this obliquity forcing, however, depends on the climatic precession. According to the CCSM3 results, the Indian monsoon is less sensitive to direct obliquity-induced insolation forcing, consistent with the interpretation of proxy records from the Arabian Sea. Moreover, the model results suggest that the two monsoon systems do not always vary in concert, challenging the concept of a global monsoon system at orbital timescales. High obliquity can also explain relatively warm Northern Hemisphere high-latitude summer temperatures despite maximum precession around 495 kyr BP (MIS 13) probably preventing a glacial inception at that time.

## 1 Introduction

The Quaternary period is characterized by the cyclic growth and decay of continental ice sheets associated with global environmental changes (e.g., Lisiecki and Raymo, 2005; Tzedakis et al., 2006; Jouzel et al., 2007; Lang and Wolff, 2011). While it is commonly accepted that the transitions between glacial and interglacial stages are ultimately triggered by varying orbital insolation (Hays et al., 1976), climate research is just beginning to understand the internal climate feedbacks that are required to shift the Earth system from one state to the other (e.g., van Nes et al., 2015). The astronomical forcing, with its characteristic periods of ca. 400 and 100 kyr (eccentricity), 41 kyr

CPD

11, 3071–3107, 2015

## Intra-interglacial climate variability from MIS 15 to the Holocene

R. Rachmayani et al.

Title Page

Abstract

Introduction

Conclusions

References

Tables

Figures



Back

Close

Full Screen / Esc

Printer-friendly Version

Interactive Discussion



## Intra-interglacial climate variability from MIS 15 to the Holocene

R. Rachmayani et al.

[Title Page](#)

[Abstract](#)

[Introduction](#)

[Conclusions](#)

[References](#)

[Tables](#)

[Figures](#)



[Back](#)

[Close](#)

[Full Screen / Esc](#)

[Printer-friendly Version](#)

[Interactive Discussion](#)



(obliquity), and ca. 19 and 23 kyr (precession), also acts as an external driver for long-term climate change within the interglacials (i.e. the long-term intra-interglacial climate variability) and likely contributes to interglacial diversity since the evolution of orbital parameters differs between all Quaternary interglacial stages (cf. Tzedakis et al., 2009).

5 Understanding both interglacial climate diversity and intra-interglacial variability helps to estimate the sensitivity of the Earth system to different forcings and to assess the rate and magnitude of current climate change relative to natural variability.

10 While the present and the last interglacial have been extensively investigated with fully coupled atmosphere–ocean general circulation models (e.g., Braconnot et al., 2007; Lunt et al., 2013), earlier interglacial periods have received much less attention by climate modellers. Coupled general circulation model (CGCM) studies of earlier interglacial climates have recently been performed for Marine Isotope Stage (MIS) 11 (Milker et al., 2013; Kleinen et al., 2014) and MIS 13 (Muri et al., 2013). Using the CGCM CCSM3 (Community Climate System Model version 3), Herold et al. (2012) 15 presented a set of interglacial climate simulations comprising the interglaciations of MIS 1, 5, 9, 11 and 19. Their study, however, focussed on peak interglacial forcing (i.e. Northern Hemisphere summer occurring at perihelion) and intercomparison of interglacials (i.e. interglacial diversity) only. Here, we present a different and complementary CGCM (CCSM3) study which takes intra-interglacial climate variability into 20 account by simulating two or more time slices for each interglacial stage of MIS 1, 5, 11, 13, and 15. The goal of this study is to disentangle the effects of obliquity, precession and greenhouse gases (GHG) on global surface climate. In contrast to previously performed climate model experiments with idealized orbital forcing, in which obliquity and precession have usually set to extreme values (e.g., Tuentner et al., 2003; Mantsis et al., 2011, 2014; Erb et al., 2013; Bosmans et al., 2015), our analyzes are based on 25 realistic orbital configurations and hence climate states. Special focus is on the sensitivity of the West African and Indian monsoon systems to obliquity and precession forcing. In particular, the applicability of the global monsoon concept (Trenberth et al., 2000; Wang et al., 2014) will be tested for orbital timescales.

## 2 Experimental setup

### 2.1 Model description

We use the fully coupled climate model CCSM3 with the atmosphere, ocean, sea-ice and land-surface components interactively connected by a flux coupler (Collins et al., 2006). We apply the low-resolution version of the model (Yeager et al., 2006) which enables us to simulate a large set of time slices. In this version, the resolution of the atmosphere is given by T31 spectral truncation (3.75° transform grid) with 26 layers, while the ocean model has a nominal horizontal resolution of 3° (as has the sea-ice component) with 25 levels in the vertical. The land model shares the same horizontal grid with the atmosphere and includes components for biogeophysics, biogeochemistry, the hydrological cycle as well as a Dynamic Global Vegetation Model (DGVM) based on the Lund–Potsdam–Jena (LPJ)-DGVM (Sitch et al., 2003; Levis et al., 2004; Bonan and Levis, 2006). The DGVM predicts the distribution of 10 plant functional types (PFT) which are differentiated by physiological, morphological, phenological, bioclimatic, and fire-response attributes (Levis et al., 2004). In order to improve the simulation of land-surface hydrology and hence the vegetation cover, new parameterizations for canopy interception and soil evaporation were implemented into the land component (Oleson et al., 2008; Handiani et al., 2013; Rachmayani et al., 2015). PFT population densities are restored annually, while the land and atmosphere models are integrated with a 30 min time step.

### 2.2 Setup of experiments

To serve as a reference climatic state, a standard pre-industrial (PI) control simulation was carried out following PMIP (Paleoclimate Modelling Intercomparison Project) guidelines with respect to the forcing (e.g., Braconnot et al., 2007). The PI boundary conditions include orbital parameters of 1950 AD, atmospheric trace gas concentrations from the 18th century (Table 1) as well as pre-industrial distributions of at-

CPD

11, 3071–3107, 2015

## Intra-interglacial climate variability from MIS 15 to the Holocene

R. Rachmayani et al.

Title Page

Abstract

Introduction

Conclusions

References

Tables

Figures



Back

Close

Full Screen / Esc

Printer-friendly Version

Interactive Discussion



mospheric ozone, sulfate aerosols, and carbonaceous aerosols (Otto-Bliesner et al., 2006). The solar constant is set to  $1365 \text{ W m}^{-2}$ . The PI control run was integrated for 1000 years starting from modern initial conditions, except for the vegetation which starts from bare soil.

In total, 13 interglacial time slice experiments were carried out, all branching off from year 600 of the PI spin-up run and running for 400 years each. Boundary conditions for the selected time slices which are spanning the last 615 kyr comprise orbital parameters (Berger, 1978) and GHG concentrations as given in Table 1, while other forcings (ice sheet configuration, ozone distribution, sulfate aerosols, carbonaceous aerosols, solar constant) were kept as in the PI control run. The mean of the last 100 simulation years of each experiment was used for analysis.

### 2.3 Selection of interglacial time slices

Our selection of interglacial time slices takes into account different aspects of inter- and intra-interglacial variability and associated astronomical forcing. As such, our approach differs from and complements previous model studies that focussed on peak interglacial forcing and intercomparison of interglacials (Yin and Berger, 2012; Herold et al., 2012).

For MIS 1, the mid-Holocene time slice of 6 kyr BP using standard PMIP forcing (Braconnot et al., 2007) was complemented by an early-Holocene 9 kyr BP simulation when Northern Hemisphere summer insolation was close to maximum (Fig. 1). Two time slices, 125 and 115 kyrBP, were also chosen for the last interglacial (MIS 5e). Similar to 9 kyrBP, the 125 kyr BP time slice is also characterized by nearly peak interglacial forcing, although the MIS 5 insolation forcing is stronger due to a greater eccentricity of the Earth's orbit. Moreover, the global benthic  $\delta^{18}\text{O}$  stack is at minimum around 125 kyr BP (Lisiecki and Raymo, 2005). By contrast, boreal summer insolation is close to minimum at 115 kyrBP, which marked the end of MIS 5e (Fig. 1). GHG concentrations for the MIS 5 time slices were taken as specified by PMIP-3 (Lunt et al., 2013).

## Intra-interglacial climate variability from MIS 15 to the Holocene

R. Rachmayani et al.

Title Page

Abstract

Introduction

Conclusions

References

Tables

Figures



Back

Close

Full Screen / Esc

Printer-friendly Version

Interactive Discussion





distribution of methane sources and sinks over the latitudes, values of atmospheric CH<sub>4</sub> concentration derived from Antarctic ice cores present a lower estimate of global CH<sub>4</sub> concentration. We further note that some results from the MIS 1 (6 and 9 kyr BP), MIS 5 (125 kyr BP), and MIS 11 (394, 405, and 416 kyr BP) experiments were previously published (Lunt et al., 2013; Milker et al., 2013; Kleinen et al., 2014; Rachmayani et al., 2015).

## 2.4 Insolation anomalies

Annual cycles of the latitudinal distribution of insolation at the top of the atmosphere (as anomalies relative to PI) are shown in Fig. 2 for each experiment. The insolation patterns can be divided into three groups which differ in their seasonal distribution of incoming energy. Group I is characterized by high Northern Hemisphere summer insolation as exhibited for the 6 and 9 kyr BP (MIS 1), 125 kyr BP (MIS 5), 405 and 416 kyr BP (MIS 11), 504 kyr BP (MIS 13), and 579 kyr BP (MIS 15) time slices. In most (but not all, see below) cases this is due to an orbital configuration with northern summer solstice at or close to perihelion. Group II comprises anomalies with low boreal summer insolation as shown for 115 kyr BP (MIS 5), 495 and 516 kyr BP (MIS 13), and 609 kyr BP (MIS 15). In these cases, northern winter solstice is near perihelion. Group III is characterized by changes in the sign of the Northern Hemisphere insolation anomalies from spring to summer and consists of two dates (394 and 615 kyr BP). At 394 (615 kyr BP) the insolation anomaly spring-to-summer change is from positive (negative) to negative (positive). In these cases, spring equinox (394 kyr BP) or fall equinox (615 kyr BP) are close to perihelion.

CPD

11, 3071–3107, 2015

### Intra-interglacial climate variability from MIS 15 to the Holocene

R. Rachmayani et al.

Title Page

Abstract

Introduction

Conclusions

References

Tables

Figures

◀

▶

◀

▶

Back

Close

Full Screen / Esc

Printer-friendly Version

Interactive Discussion



### 3 Results

#### 3.1 JJAS surface temperature anomalies

The response of boreal summer (June–July–August–September, JJAS) surface temperature to the combined effect of insolation and GHG in all individual climates (Fig. 3) shows warm conditions (relative to PI) over most parts of the continents in Group I (6, 9, 125, 405, 416, 504, and 579 kyrBP) with the three warmest anomalies at 9, 125, and 579 kyrBP. The warm surface conditions can largely be explained by the immediate effect of high summer insolation and a reduction of the Northern Hemisphere sea-ice area by about 15–20% (not shown) relative to PI. The large thermal capacity of the ocean explains a larger temperature response over land than over the ocean (Herold et al., 2012; Nikolova et al., 2013). Simulated cooling over North Africa (10–25° N) and India in the Group I experiments is caused by enhanced monsoonal rainfall in these regions, which is associated with increased cloud cover, i.e. reduced short-wave fluxes, and enhanced land surface evapotranspiration, i.e. greater latent cooling (e.g., Braconnot et al., 2002, 2004; Zheng and Braconnot, 2013). The 416 kyr BP time slice, however, differs from the other Group I members by anomalously cold conditions over the Southern Hemisphere continents. Again, this behaviour can be explained by the immediate effect of the insolation, which shows negative anomalies in the Southern Hemisphere during the JJAS season (Fig. 2). As such, the 416 kyrBP time slice must be considered a special case in Group I. While high Northern Hemisphere summer insolation is related to low precession in most Group I members, positive anomalies of Northern Hemisphere summer insolation at 416 kyr BP are attributable to a maximum in obliquity (Fig. 1), yielding the Northern-versus-Southern Hemisphere insolation contrast.

In contrast to Group I, Group II climates exhibit anomalously cold JJAS surface temperatures globally with the three coldest anomalies at 115, 516, and 609 kyrBP. Again, the temperature response can largely be explained by the direct response to insolation forcing, amplified in high latitudes by an increase of the sea-ice cover (about 5% in the

CPD

11, 3071–3107, 2015

## Intra-interglacial climate variability from MIS 15 to the Holocene

R. Rachmayani et al.

Title Page

Abstract

Introduction

Conclusions

References

Tables

Figures



Back

Close

Full Screen / Esc

Printer-friendly Version

Interactive Discussion









anomaly is extremely high in this experiment (Fig. 7a). During boreal winter, Northern Hemisphere continents show large-scale cooling in response to high obliquity (and hence relatively low insolation), except for the Arctic realm where the summer remnant effect results in substantial positive surface temperature anomalies (Fig. 8c and d).

During the same season (DJF) anomalously high insolation causes surface warming in the Southern Hemisphere in response to high obliquity.

As a general pattern, especially in the annual mean, maximum-minus-minimum obliquity insolation anomalies cause anomalous surface warming at high latitudes and surface cooling at low latitudes. Aside from seasonal insolation anomalies and climate feedbacks (polar summer remnant effect, monsoons) that create this general pattern, it is also consistent with the obliquity effect on annual insolation, which implies higher annual insolation at the poles and lower annual insolation (but to a lesser extent) at the equator.

Despite the weak insolation signal at low latitudes, substantial obliquity-induced changes in tropical precipitation are simulated (Fig. 8e and f). The strongest signal is found in the North African monsoon region in the MIS 11 experiments, where greater JJAS precipitation occurs during maximum obliquity at 416 kyr BP than during the obliquity minimum at 394 kyr BP. A positive Sahel rainfall anomaly is also found in the MIS 13 experiments (495–516 kyr BP), but much weaker than in the MIS 11 case (416–394 kyr BP). We suppose that the obliquity-induced increase in North African monsoonal rainfall is counteracted by the high precession at 495 kyr BP that tends to weaken the monsoon.

### 3.6 Evaluating the climatic effects of astronomical and GHG forcings through correlation maps

In order to evaluate the climatic effects of obliquity, precession and GHG concentrations, linear correlations between the individual forcing parameters and climatic fields (surface temperature, precipitation) were calculated from the 14 time slice experiments (13 interglacial time slices plus PI). To this end, the total radiative forcing from CO<sub>2</sub>,

## Intra-interglacial climate variability from MIS 15 to the Holocene

R. Rachmayani et al.

Title Page

Abstract

Introduction

Conclusions

References

Tables

Figures



Back

Close

Full Screen / Esc

Printer-friendly Version

Interactive Discussion



CH<sub>4</sub>, and N<sub>2</sub>O in each experiment was calculated based on a simplified expression (IPCC, 2001).

Figure 9 shows the corresponding correlation maps for annual mean, boreal summer, and boreal winter surface temperature. As expected, GHG forcing is positively correlated with surface temperature over most regions of the globe (Fig. 9a), which is particularly pronounced in the annual mean. For the seasonal correlation maps (boreal summer and winter) the correlation coefficients are smaller because of the dominant impact of obliquity and precession forcing. As already described in the previous subsection, the general surface temperature pattern of high obliquity forcing is warming at high latitudes and cooling at low latitudes (Fig. 9b). High precession (northern solstice near aphelion) leads to boreal summer surface cooling over most extratropical regions (Fig. 9c). However, surface warming occurs in tropical regions as a response to weaker monsoons. During boreal winter, anomalously high insolation causes anomalous surface warming except in the Arctic (due to the summer remnant effect) and northern Australia (due to a stronger regional monsoon).

Correlation maps for annual mean, boreal summer, and boreal winter precipitation are shown in Fig. 10. GHG radiative forcing exhibits no clear response in precipitation except for the high latitudes where the hydrologic cycle accelerates with higher GHG concentrations (Fig. 10a). Arctic precipitation is also amplified by high obliquity during summer (Fig. 10b). Obliquity also strengthens the monsoonal rainfall in North Africa (Sahel region), whereas no effect of obliquity can be detected for the Australian monsoon. The most robust response of the hydrologic cycle is found for precession (Fig. 10c). In particular, high precession reduces summer rainfall in the monsoon belt from North Africa to India as well as in the Arctic realm. During boreal winter, the hydrologic cycle strengthens in the Arctic and Antarctic regions, while Southern Hemisphere monsoon systems amplify resulting in enhanced rainfall over South America, southern Africa, and northern Australia in response to high precession.

## Intra-interglacial climate variability from MIS 15 to the Holocene

R. Rachmayani et al.

[Title Page](#)[Abstract](#)[Introduction](#)[Conclusions](#)[References](#)[Tables](#)[Figures](#)[Back](#)[Close](#)[Full Screen / Esc](#)[Printer-friendly Version](#)[Interactive Discussion](#)







**Intra-interglacial  
climate variability  
from MIS 15 to the  
Holocene**

R. Rachmayani et al.

[Title Page](#)[Abstract](#)[Introduction](#)[Conclusions](#)[References](#)[Tables](#)[Figures](#)[Back](#)[Close](#)[Full Screen / Esc](#)[Printer-friendly Version](#)[Interactive Discussion](#)

is found that the two monsoon systems do not always vary in concert. This is particularly evident in the Group III experiments (394 and 615 kyr BP) where the precipitation anomalies over North Africa and India have opposite signs (Table 2). Considering the annual insolation cycle in these experiments (Fig. 2), the West African monsoon turns out to be forced by summer insolation, whereas spring/early summer insolation is more important for the Indian monsoon. The different responses to specific forcings and the sometimes out-of-phase behaviour of the African and Indian monsoon systems challenge the global monsoon concept – according to which all regional monsoon systems are part of one seasonally varying global-scale atmospheric overturning circulation in the tropics (Trenberth et al., 2000; Wang et al., 2014) – at orbital timescales.

## 5 Conclusions

Using a state-of-the-art CGCM, 13 interglacial time slice experiments were carried out to study global climate variability between and within Quaternary interglacials. The different roles of obliquity, precession and GHG forcing on surface temperature and precipitation patterns have been disentangled. Several similarities with previous idealized orbital-forcing experiments could be identified. In particular, a significant role of obliquity in forcing the West African monsoon was found, whereas the Indian monsoon appears to be less sensitive to obliquity changes. Different responses to specific forcings and the obvious anti-phase behaviour of the African and Indian monsoon systems in the 394 and 615 kyr BP experiments challenge the global monsoon concept. High obliquity can also explain relatively warm Northern Hemisphere high-latitude summer temperatures despite maximum precession at 495 kyr BP (MIS 13) probably preventing a glacial inception at that time.

Future studies should include the effects of changing ice sheets and associated melt-water fluxes in shaping interglacial climates. Large Northern Hemisphere ice sheets might have played an important role for regional and global climates especially during early Brunhes interglacials (MIS 13 and before) as suggested by, e.g., Yin et al.



## Intra-interglacial climate variability from MIS 15 to the Holocene

R. Rachmayani et al.

Title Page

Abstract

Introduction

Conclusions

References

Tables

Figures



Back

Close

Full Screen / Esc

Printer-friendly Version

Interactive Discussion



- Bosmans, J. H. C., Drijfhout, S. S., Tuentler, E., Hilgen, F. J., and Lourens, L. J.: Response of the North African summer monsoon to precession and obliquity forcings in the EC-Earth GCM, *Clim. Dynam.*, 44, 279–297, doi:10.1007/s00382-014-2260-z, 2015. 3073, 3085, 3086
- Braconnot, P., Loutre, M. F., Dong, B., Joussaume, S., and Valdes, P.: How the simulated change in monsoon at 6 kaBP is related to the simulation of the modern climate: results from the Paleoclimate Modeling Intercomparison Project, *Clim. Dynam.*, 19, 107–121, 2002. 3078
- Braconnot, P., Harrison, S., Joussaume, J., Hewitt, C., Kitoh, A., Kutzbach, J., Liu, Z., Otto-Bliesner, B. L., Syktus, J., and Weber, S. L.: Evaluation of coupled ocean-atmosphere simulations of the mid-Holocene, in: *Past Climate Variability Through Europe and Africa*, edited by: Battarbee, R. W., Gasse, F., and Stickley, C. E., Kluwer Academic Publisher, 515–533, Dordrecht, 2004. 3078
- Braconnot, P., Otto-Bliesner, B., Harrison, S., Joussaume, S., Peterchmitt, J.-Y., Abe-Ouchi, A., Crucifix, M., Driesschaert, E., Fichet, Th., Hewitt, C. D., Kageyama, M., Kitoh, A., Laîné, A., Loutre, M.-F., Marti, O., Merkel, U., Ramstein, G., Valdes, P., Weber, S. L., Yu, Y., and Zhao, Y.: Results of PMIP2 coupled simulations of the Mid-Holocene and Last Glacial Maximum – Part 1: experiments and large-scale features, *Clim. Past*, 3, 261–277, doi:10.5194/cp-3-261-2007, 2007. 3073, 3074, 3075, 3080, 3084
- Collins, W. D., Bitz, C. M., Blackmon, M. L., Bonan, G. B., Bretherton, C. S., Carton, J. A., Chang, P., Doney, S. C., Hack, J. J., Henderson, T. B., Kiehl, J. T., Large, W. G., McKenna, D. S., Santer, B. D., and Smith, R. D.: The Community Climate System Model version 3 (CCSM3), *J. Climate*, 19, 2122–2143, doi:10.1175/JCLI3761.1, 2006. 3074
- Davis, B. A. S. and Brewer, S.: Orbital forcing and role of the Latitudinal Insolation/Temperature Gradient, *Clim. Dynam.*, 32, 143–165, doi:10.1007/s00382-008-0480-9, 2009. 3086
- deMenocal, P. B.: Plio-Pleistocene African climate, *Science*, 270, 53–59, doi:10.1126/science.270.5233.53, 1995. 3086
- deMenocal, P. B., Ruddiman, W. F., and Pokras, E. K.: Influences of high- and low-latitude processes on African climate: Pleistocene eolian records from equatorial Atlantic Ocean Drilling Program Site 663, *Paleoceanography*, 8, 209–242, doi:10.1029/93PA02688, 1993. 3086
- de Noblet, N., Braconnot, P., Joussaume, S., and Masson, V.: Sensitivity of simulated Asian and African boreal summer monsoons to orbitally induced variations in insolation 126, 115 and 6 kaBP, *Clim. Dynam.*, 12, 589–603, 1996. 3080

## Intra-interglacial climate variability from MIS 15 to the Holocene

R. Rachmayani et al.

Title Page

Abstract

Introduction

Conclusions

References

Tables

Figures



Back

Close

Full Screen / Esc

Printer-friendly Version

Interactive Discussion



- Erb, M. P., Broccoli, A. J., and Clement, A. C.: The contribution of radiative feedbacks to orbitally driven climate change, *J. Climate*, 26, 5897–5914, 2013. 3073, 3076, 3085
- Fischer, N. and Jungclaus, J. H.: Effects of orbital forcing on atmosphere and ocean heat transports in Holocene and Eemian climate simulations with a comprehensive Earth system model, *Clim. Past*, 6, 155–168, doi:10.5194/cp-6-155-2010, 2010. 3079
- 5 Fleitmann, D., Burns, S. J., Mudelsee, M., Neff, U., Kramers, J., Mangini, A., and Matter, A.: Holocene forcing of the Indian monsoon recorded in a stalagmite from Southern Oman, *Science*, 300, 1737–1739, 2003. 3084
- Gallimore, R. G. and Kutzbach, J. E.: Role of orbitally induced changes in tundra area in the onset of glaciation, *Nature*, 381, 503–505, 1996. 3084
- 10 Govin, A., Varma, V., and Prange, M.: Astronomically forced variations in western African rainfall (21° N–20° S) during the Last Interglacial period, *Geophys. Res. Lett.*, 41, 2117–2125, doi:10.1002/2013GL058999, 2014. 3088
- Handiani, D., Paul, A., Prange, M., Merkel, U., Dupont, L., and Zhang, X.: Tropical vegetation response to Heinrich Event 1 as simulated with the UVic ESCM and CCSM3, *Clim. Past*, 9, 1683–1696, doi:10.5194/cp-9-1683-2013, 2013. 3074
- 15 Hays, J. D., Imbrie, J., and Shackleton, N. J.: Variations in the Earth's orbit: pacemaker of the Ice Ages, *Science*, 194, 1121–1132, 1976. 3072
- Herold, N., Yin, Q. Z., Karami, M. P., and Berger, A.: Modelling the climatic diversity of the warm interglacials, *Quaternary Sci. Rev.*, 56, 126–141, doi:10.1016/j.quascirev.2012.08.020, 2012. 3073, 3075, 3078, 3079
- 20 Hessler, I., Harrison, S. P., Kucera, M., Waelbroeck, C., Chen, M.-T., Anderson, C., de Vernal, A., Fréchet, B., Cloke-Hayes, A., Leduc, G., and Londeix, L.: Implication of methodological uncertainties for mid-Holocene sea surface temperature reconstructions, *Clim. Past*, 10, 2237–2252, doi:10.5194/cp-10-2237-2014, 2014. 3085
- 25 Hoelzmann, P., Jolly, D., Harrison, S. P., Laarif, F., Bonnefille, R., and Pachur, H. J.: Mid-Holocene land surface conditions in northern Africa and the Arabian Peninsula: a data set for the analysis of biogeochemical feedbacks in the climate system, *Global Biogeochem. Cy.*, 12, 35–52, 1998. 3084
- 30 Jochum, M., Jahn, A., Peacock, S., Bailey, D. A., Fasullo, J. T., Kay, J., Levis, S., and Otto-Bliesner, B.: True to Milankovitch: glacial inception in the new Community Climate System Model, *J. Climate*, 25, 2226–2239, doi:10.1175/JCLI-D-11-00044.1, 2012. 3084

## Intra-interglacial climate variability from MIS 15 to the Holocene

R. Rachmayani et al.

[Title Page](#)

[Abstract](#)

[Introduction](#)

[Conclusions](#)

[References](#)

[Tables](#)

[Figures](#)



[Back](#)

[Close](#)

[Full Screen / Esc](#)

[Printer-friendly Version](#)

[Interactive Discussion](#)

- Jouzel, J., Masson-Delmotte, V., Cattani, O., Dreyfus, G., Falourd, S., Hoffmann, G., Minster, B., Nouet, J., Barnola, J. M., Chappellaz, J., Fischer, H., Gallet, J. C., Johnsen, S., Leuenberger, M., Loulergue, L., Luethi, D., Oerter, H., Parrenin, F., Raisbeck, G., Raynaud, D., Schilt, A., Schwander, J., Selmo, E., Souchez, R., Spahni, R., Stauffer, B., Steffensen, J. P., Stenni, B., Stocker, T. F., Tison, J. L., Werner, M., and Wolff, E. W.: Climate variability over the past 800 000 years, *Science*, 317, 793–796, doi:10.1126/science.1141038, Data archived at the World Data Center for Paleoclimatology, Boulder, Colorado, USA, 2007. 3072
- Kaspar, F. and Cubasch, U.: Simulation of the Eemian interglacial and possible mechanisms for the glacial inception, *Geol. S. Am. S.*, 426, 29–41, 2007. 3084
- Khodri, M., Cane, M. A., Kukla, G., Gavin, J., and Braconnot, P.: The impact of precession changes on the Arctic climate during the last interglacial-glacial transition, *Earth Planet. Sc. Lett.*, 236, 285–304, 2005. 3084
- Kleinen, T., Hildebrandt, S., Prange, M., Rachmayani, R., Müller, S., Bezrukova, S., Brovkin, V., and Tarasov, P.: The climate and vegetation of Marine Isotope Stage 11 - model results and proxy-based reconstructions at global and regional scale, *Quatern. Int.*, 348, 247–265, doi:10.1016/j.quaint.2013.12.028, 2014. 3073, 3077, 3079, 3085
- Kroon, D., Alexander, I., Little, M., Lourens, L. J., Matthewson, A., Robertson, A. H., and Sakamoto, T.: Oxygen isotope and sapropel stratigraphy in the eastern Mediterranean during the last 3.2 million years, *Proceedings of the Ocean Drilling Program, Scientific Results*, 160, 181–189, 1998. 3086
- Lang, N. and Wolff, E. W.: Interglacial and glacial variability from the last 800 kyr in marine, ice and terrestrial archives, *Clim. Past*, 7, 361–380, doi:10.5194/cp-7-361-2011, 2011. 3072
- Levis, S., Bonan, G. B., Vertenstein, M., and Oleson, K. W.: The Community Land Models Dynamic Global Vegetation Model (CLM-DGVM): Technical Description and User's Guide, NCAR Technical Note NCAR/TN-459+IA, National Center for Atmospheric Research, Boulder, CO, 2004. 3074
- Lisiecki, L. E. and Raymo, M. E.: A Pliocene-Pleistocene stack of 57 globally distributed benthic  $\delta^{18}\text{O}$  records, *Paleoceanography*, 20, PA1003, doi:10.1029/2004PA001071, 2005. 3072, 3075, 3076, 3085, 3098
- Liu, Z., Zhu, J., Rosenthal, Y., Zhang, X., Otto-Bliesner, B. L., Timmermann, A., Smith, R. S., Lohmann, G., Zheng, W., and Timm, O. E.: The Holocene temperature conundrum, *P. Natl. Acad. Sci. USA*, 111, E3501–E3505, doi:10.1073/pnas.1407229111, 2014. 3085, 3088

**Intra-interglacial  
climate variability  
from MIS 15 to the  
Holocene**

R. Rachmayani et al.

[Title Page](#)[Abstract](#)[Introduction](#)[Conclusions](#)[References](#)[Tables](#)[Figures](#)[Back](#)[Close](#)[Full Screen / Esc](#)[Printer-friendly Version](#)[Interactive Discussion](#)

Lohmann, G., Pfeiffer, M., Laepple, T., Leduc, G., and Kim, J.-H.: A model–data comparison of the Holocene global sea surface temperature evolution, *Clim. Past*, 9, 1807–1839, doi:10.5194/cp-9-1807-2013, 2013. 3085

Lorenz, S. J. and Lohmann, G.: Acceleration technique for Milankovitch type forcing in a coupled atmosphere–ocean circulation model: method and application for the Holocene, *Clim. Dynam.*, 23, 727–743, 2004. 3088

Loulergue, L., Schilt, A., Spahni, R., Masson-Delmotte, V., Blunier, T., Lemieux, B., Barnola, J.-M., Raynaud, D., Stocker, T. F., and Chappellaz, J.: Orbital and millennial-scale features of atmospheric CH<sub>4</sub> over the past 800,000 years, *Nature*, 453, 383–386, 2008. 3076

Lunt, D. J., Abe-Ouchi, A., Bakker, P., Berger, A., Braconnot, P., Charbit, S., Fischer, N., Herold, N., Jungclaus, J. H., Khon, V. C., Krebs-Kanzow, U., Langebroek, P. M., Lohmann, G., Nisancioglu, K. H., Otto-Bliesner, B. L., Park, W., Pfeiffer, M., Phipps, S. J., Prange, M., Rachmayani, R., Renssen, H., Rosenbloom, N., Schneider, B., Stone, E. J., Takahashi, K., Wei, W., Yin, Q., and Zhang, Z. S.: A multi-model assessment of last interglacial temperatures, *Clim. Past*, 9, 699–717, doi:10.5194/cp-9-699-2013, 2013. 3073, 3075, 3077, 3084, 3085

Lüthi, D., Le Floch, M., Bereiter, B., Blunier, T., Barnola, J.-M., Siegenthaler, U., Raynaud, D., Jouzel, J., Fischer, H., Kawamura, K., and Stocker, T. F.: High-resolution carbon dioxide concentration record 650,000–800,000 years before present, *Nature*, 453, 379–382, 2008. 3076

Mantsis, D. F., Clement, A. C., Broccoli, A. J., and Erb, M. P.: Climate feedbacks in response to changes in obliquity, *J. Climate*, 24, 2830–2845, 2011. 3073, 3076, 3085

Mantsis, D. F., Lintner, B. R., Broccoli, A. J., Erb, M. P., Clement, A. C., and Park, H. S.: The response of large-scale circulation to obliquity-induced changes in meridional heating gradients, *J. Climate*, 27, 5504–5516, 2014. 3073, 3076

Marzin, C., Braconnot, P., and Kageyama, M.: Relative impacts of insolation changes, meltwater fluxes and ice sheets on African and Asian monsoons during the Holocene, *Clim. Dynam.*, 41, 2267–2286, 2013. 3088

McClure, H. A.: Radiocarbon chronology of late Quaternary lakes in the Arabian Desert, *Nature*, 263, 755–756, 1976. 3084

Meissner, K. J., Weaver, A. J., Matthews, H. D., and Cox, P. M.: The role of land-surface dynamics in glacial inception: a study with the UVic Earth System Climate Model, *Clim. Dynam.*, 21, 519–537, 2003. 3084

**Intra-interglacial  
climate variability  
from MIS 15 to the  
Holocene**

R. Rachmayani et al.

[Title Page](#)[Abstract](#)[Introduction](#)[Conclusions](#)[References](#)[Tables](#)[Figures](#)[Back](#)[Close](#)[Full Screen / Esc](#)[Printer-friendly Version](#)[Interactive Discussion](#)

- Milker, Y., Rachmayani, R., Weinkauf, M. F. G., Prange, M., Raitzsch, M., Schulz, M., and Kučera, M.: Global and regional sea surface temperature trends during Marine Isotope Stage 11, *Clim. Past*, 9, 2231–2252, doi:10.5194/cp-9-2231-2013, 2013. 3073, 3076, 3077, 3085
- Muri, H., Berger, A., Yin, Q., Karami, M., and Barriat, P. V.: The climate of the MIS-13 Interglacial according to HadCM3, *J. Climate*, 26, 9696–9712, 2013. 3073, 3084, 3088
- Nikolova, I., Yin, Q., Berger, A., Singh, U. K., and Karami, M. P.: The last interglacial (Eemian) climate simulated by LOVECLIM and CCSM3, *Clim. Past*, 9, 1789–1806, doi:10.5194/cp-9-1789-2013, 2013. 3078
- Oleson, K. W., Niu, G. Y., Yang, Z. L., Lawrence, D. M., Thornton, P. E., Lawrence, P. J., Stockli, R., Dickinson, R. E. G., Bonan, B., Levis, S., Dai, A., and Qian, T.: Improvements to the Community Land Model and their impact on the hydrological cycle, *J. Geophys. Res.*, 113, G01021, doi:10.1029/2007JG000563, 2008. 3074
- Otto-Bliesner, B. L., Tomas, R., Brady, E. C., Ammann, C., Kothavala, Z., and Clauzet, G.: Climate sensitivity of moderate and low-resolution versions of CCSM3 to preindustrial forcings, *J. Climate*, 19, 2567–2583, 2006. 3075
- Prell, W. L. and Kutzbach, J. E.: Monsoon variability over the past 150,000 years, *J. Geophys. Res.*, 92, 8411–8425, 1987. 3080
- Rachmayani, R., Prange, M., and Schulz, M.: North African vegetation–precipitation feedback in early and mid-Holocene climate simulations with CCSM3-DGVM, *Clim. Past*, 11, 175–185, doi:10.5194/cp-11-175-2015, 2015. 3074, 3077, 3080
- Renssen, H., Seppä, H., Heiri, O., Roche, D. M., Goosse, H., and Fichet, T.: The spatial and temporal complexity of the Holocene thermal maximum, *Nat. Geosci.*, 2, 411–414, 2009. 3088
- Schilt, A., Baumgartner, M., Blunier, T., Schwander, J., Spahni, R., Fischer, H., and Stocker, T. F.: Glacial–interglacial and millennial–scale variations in the atmospheric nitrous oxide concentration during the last 800,000 years, *Quaternary Sci. Rev.*, 29, 182–192, 2010. 3076
- Sitch, S., Smith, B., Prentice, I. C., Arneeth, A., Bondeau, A., Cramer, W., Kaplan, J. O., Levis, S., Lucht, W., Sykes, M. T., Thonicke, K., and Venevsky, S.: Evaluation of ecosystem dynamics, plant geography and terrestrial carbon cycling in the LPJ dynamic vegetation model, *Glob. Change Biol.*, 9, 161–185, 2003. 3074

**Intra-interglacial  
climate variability  
from MIS 15 to the  
Holocene**

R. Rachmayani et al.

[Title Page](#)[Abstract](#)[Introduction](#)[Conclusions](#)[References](#)[Tables](#)[Figures](#)[Back](#)[Close](#)[Full Screen / Esc](#)[Printer-friendly Version](#)[Interactive Discussion](#)

- Tiedemann, R., Sarnthein, M., and Shackleton, N. J.: Astronomic timescale for the Pliocene Atlantic  $\delta^{18}\text{O}$  and dust flux records of Ocean Drilling Program Site 659, *Paleoceanography*, 9, 619–638, 1994. 3086
- Trenberth, K. E., Stepaniak, D. P., and Caron, J. M.: The global monsoon as seen through the divergent atmospheric circulation, *J. Climate*, 13, 3969–3993, 2000. 3073, 3087
- Tuenter, E., Weber, S., Hilgen, F., and Lourens, L.: The response of the African boreal summer monsoon to remote and local forcing due to precession and obliquity, *Global Planet. Change*, 36, 219–235, 2003. 3073, 3076, 3080, 3085, 3086
- Tzedakis, P. C., Hooghiemstra, H., and Palike, H.: The last 1.35 million years at Tenaghi Philippon: revised chronostratigraphy and long-term vegetation trends, *Quaternary Sci. Rev.*, 25, 3416–3430, 2006. 3072
- Tzedakis, P. C., Raynaud, D., McManus, J. F., Berger, A., Brovkin, V., and Kiefer, T.: Interglacial diversity, *Nat. Geosci.*, 2, 751–755, 2009. 3073
- van Nes, E. H., Scheffer, M., Brovkin, V., Lenton, T. M., Ye, H., Deyle, E., and Sugihara, G.: Causal feedbacks in climate change, *Nature Climate Change*, 5, 445–448, doi:10.1038/nclimate2568, 2015. 3072
- Varma, V., Prange, M., Merkel, U., Kleinen, T., Lohmann, G., Pfeiffer, M., Renssen, H., Wagner, A., Wagner, S., and Schulz, M.: Holocene evolution of the Southern Hemisphere westerly winds in transient simulations with global climate models, *Clim. Past*, 8, 391–402, doi:10.5194/cp-8-391-2012, 2012. 3088
- Wang, P. X., Wang, B., Cheng, H., Fasullo, J., Guo, Z. T., Kiefer, T., and Liu, Z. Y.: The global monsoon across timescales: coherent variability of regional monsoons, *Clim. Past*, 10, 2007–2052, doi:10.5194/cp-10-2007-2014, 2014. 3073, 3087
- Yeager, S. G., Shields, C. A., Large, W. G., and Hack, J. J.: The low-resolution CCSM3, *J. Climate*, 19, 2545–2566, 2006. 3074
- Yin, Q. Z. and Berger, A.: Individual contribution of insolation and  $\text{CO}_2$  to the interglacial climates of the past 800,000 years, *Clim. Dynam.*, 38, 709–724, 2012. 3075, 3079
- Yin, Q., Berger, A., Driesschaert, E., Goosse, H., Loutre, M. F., and Crucifix, M.: The Eurasian ice sheet reinforces the East Asian summer monsoon during the interglacial 500 000 years ago, *Clim. Past*, 4, 79–90, doi:10.5194/cp-4-79-2008, 2008. 3087
- Yin, Q. Z., Berger, A., and Crucifix, M.: Individual and combined effects of ice sheets and precession on MIS-13 climate, *Clim. Past*, 5, 229–243, doi:10.5194/cp-5-229-2009, 2009. 3076

## CPD

11, 3071–3107, 2015

### Intra-interglacial climate variability from MIS 15 to the Holocene

R. Rachmayani et al.

[Title Page](#)

[Abstract](#)

[Introduction](#)

[Conclusions](#)

[References](#)

[Tables](#)

[Figures](#)



[Back](#)

[Close](#)

[Full Screen / Esc](#)

[Printer-friendly Version](#)

[Interactive Discussion](#)



## Intra-interglacial climate variability from MIS 15 to the Holocene

R. Rachmayani et al.

**Table 1.** Atmospheric GHG concentrations used in the interglacial experiments.

Stage	Time slice (kyrBP)	CO <sub>2</sub> (ppmv)	CH <sub>4</sub> (ppbv)	N <sub>2</sub> O (ppbv)
MIS 1	0	280	760	270
	6	280	650	270
	9	265	680	260
MIS 5	115	273	472	251
	125	276	640	263
MIS 11	394	275	550	275
	405	280	660	285
	416	275	620	270
MIS 13	495	240	487	249
	504	240	525	278
	516	250	500	285
MIS 15	579	252	618	266
	609	259	583	274
	615	253	617	274

Title Page

Abstract

Introduction

Conclusions

References

Tables

Figures



Back

Close

Full Screen / Esc

Printer-friendly Version

Interactive Discussion





## Intra-interglacial climate variability from MIS 15 to the Holocene

R. Rachmayani et al.

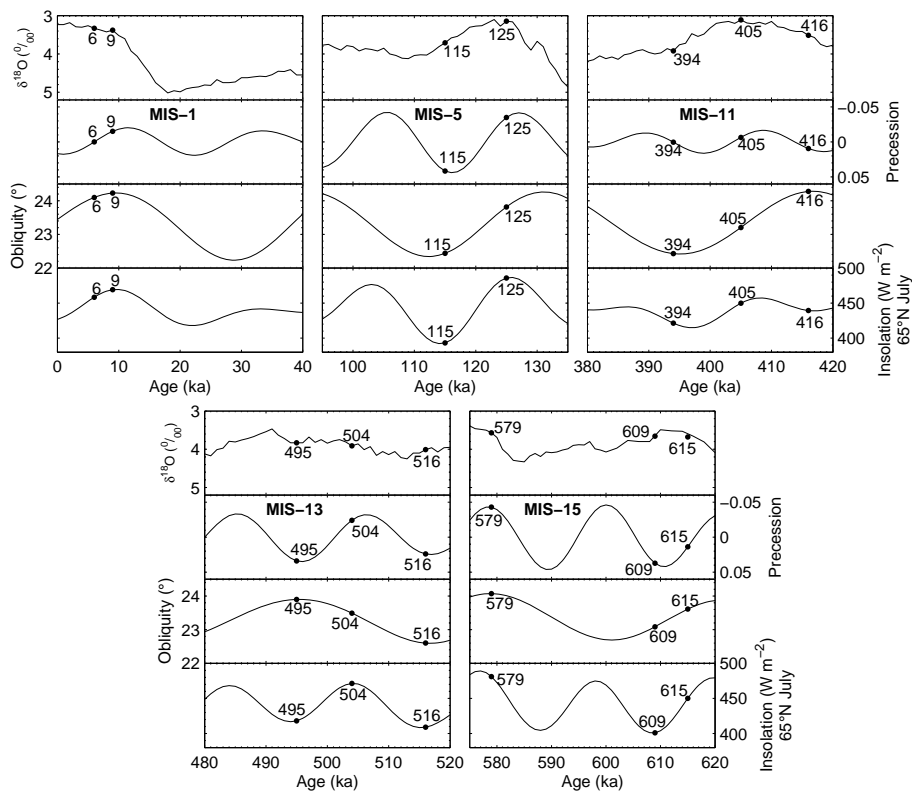


**Figure 1.** Benthic  $\delta^{18}\text{O}$  stack (Lisiecki and Raymo, 2005), climatic precession, obliquity, and insolation at July, 65°N (Berger, 1978) for the different interglacials. The points mark the time slices simulated in this study.

## Intra-interglacial climate variability from MIS 15 to the Holocene

R. Rachmayani et al.

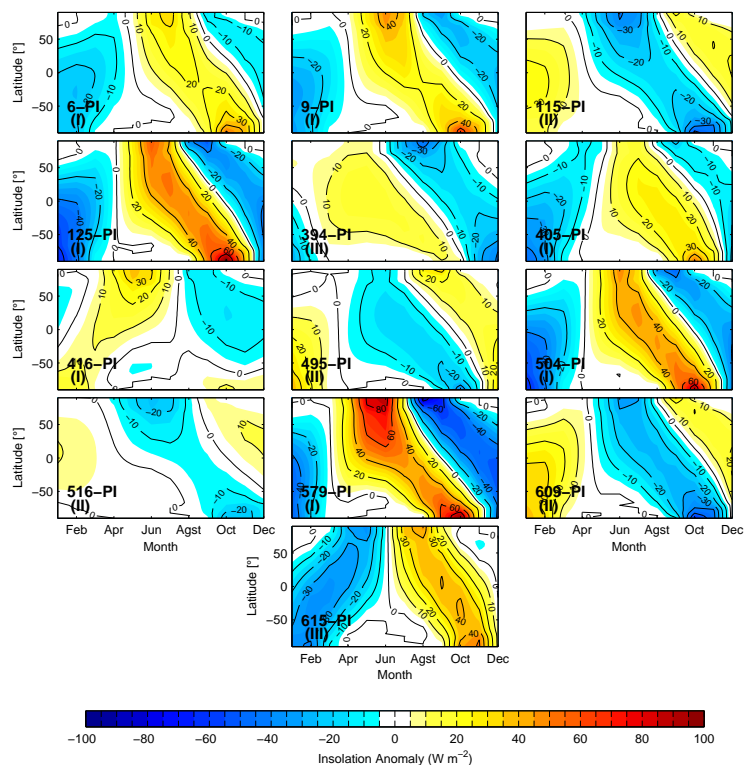


**Figure 2.** Insolation anomalies (relative to PI) for the time slices simulated in this study. Patterns of insolation anomaly are classified into Groups I, II, and III (see text). The calculation assumes a fixed present-day calendar with vernal equinox at 21 March.

[Title Page](#)
[Abstract](#)
[Introduction](#)
[Conclusions](#)
[References](#)
[Tables](#)
[Figures](#)
[Back](#)
[Close](#)
[Full Screen / Esc](#)
[Printer-friendly Version](#)
[Interactive Discussion](#)

## Intra-interglacial climate variability from MIS 15 to the Holocene

R. Rachmayani et al.

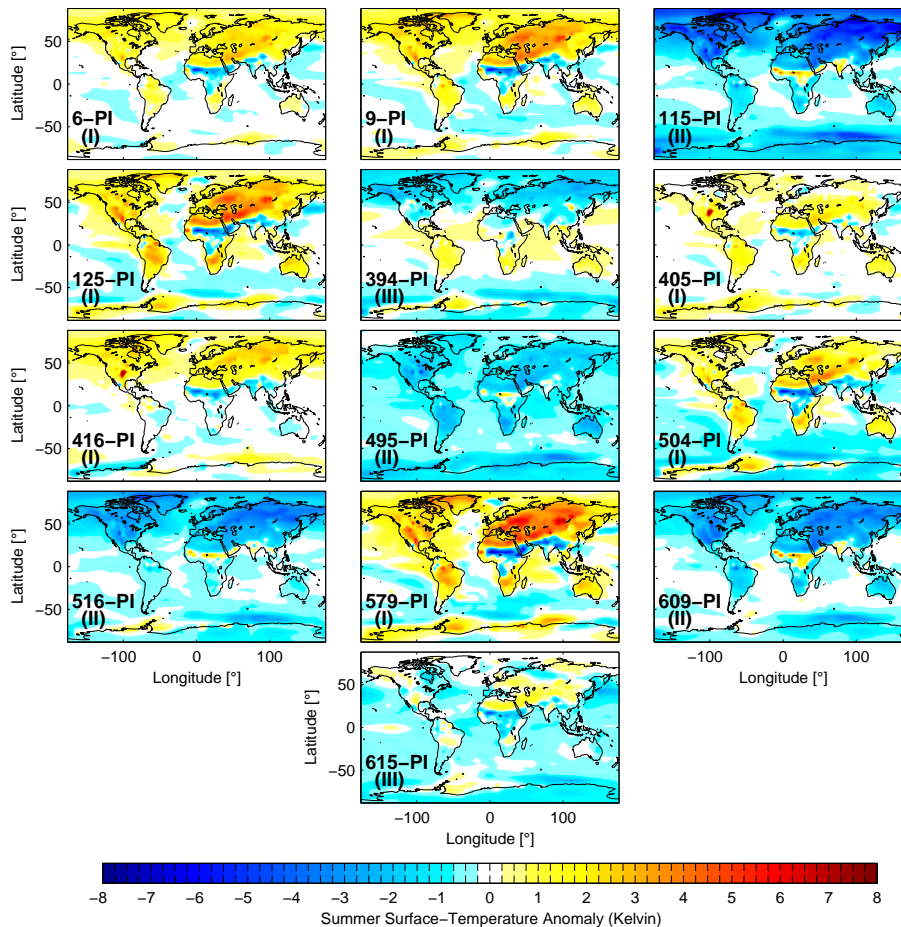


**Figure 3.** Boreal summer surface temperature anomalies (relative to PI) for the different interglacial time slices. Classification into Groups I, II, and III (see text) is indicated.

**Intra-interglacial climate variability from MIS 15 to the Holocene**

R. Rachmayani et al.

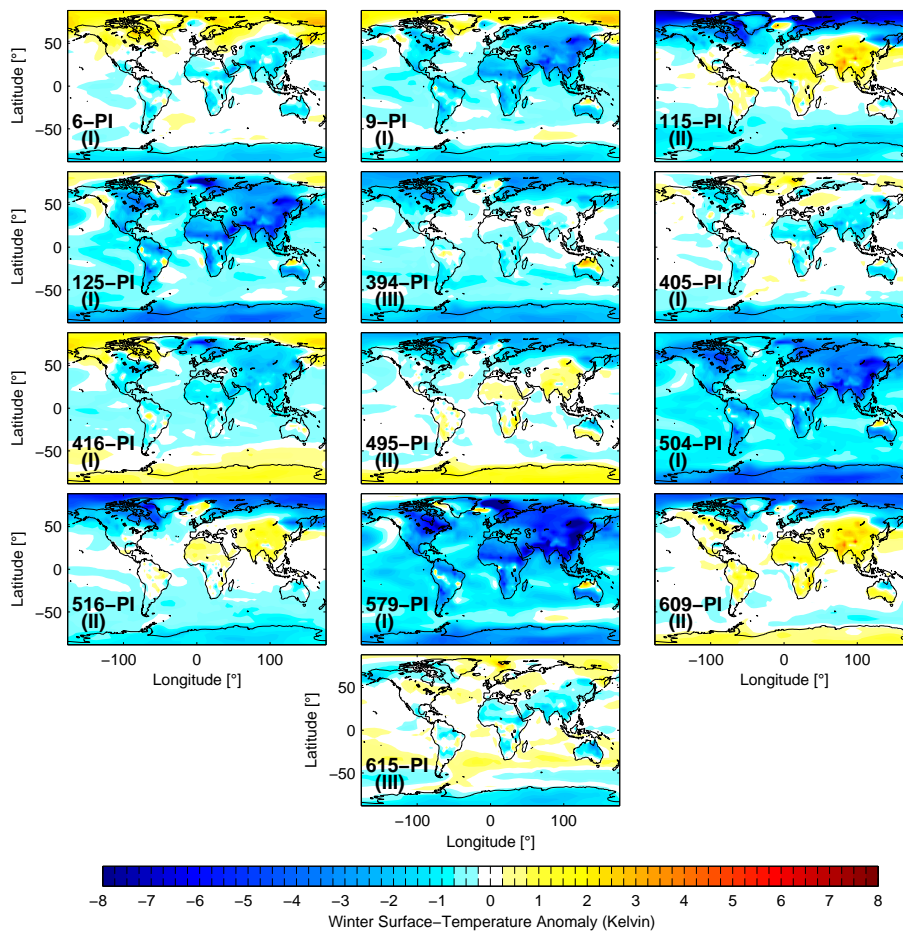


**Figure 4.** As in Fig. 3, but for boreal winter.

[Title Page](#)

[Abstract](#) | [Introduction](#)

[Conclusions](#) | [References](#)

[Tables](#) | [Figures](#)

[◀](#) | [▶](#)

[◀](#) | [▶](#)

[Back](#) | [Close](#)

[Full Screen / Esc](#)

[Printer-friendly Version](#)

[Interactive Discussion](#)



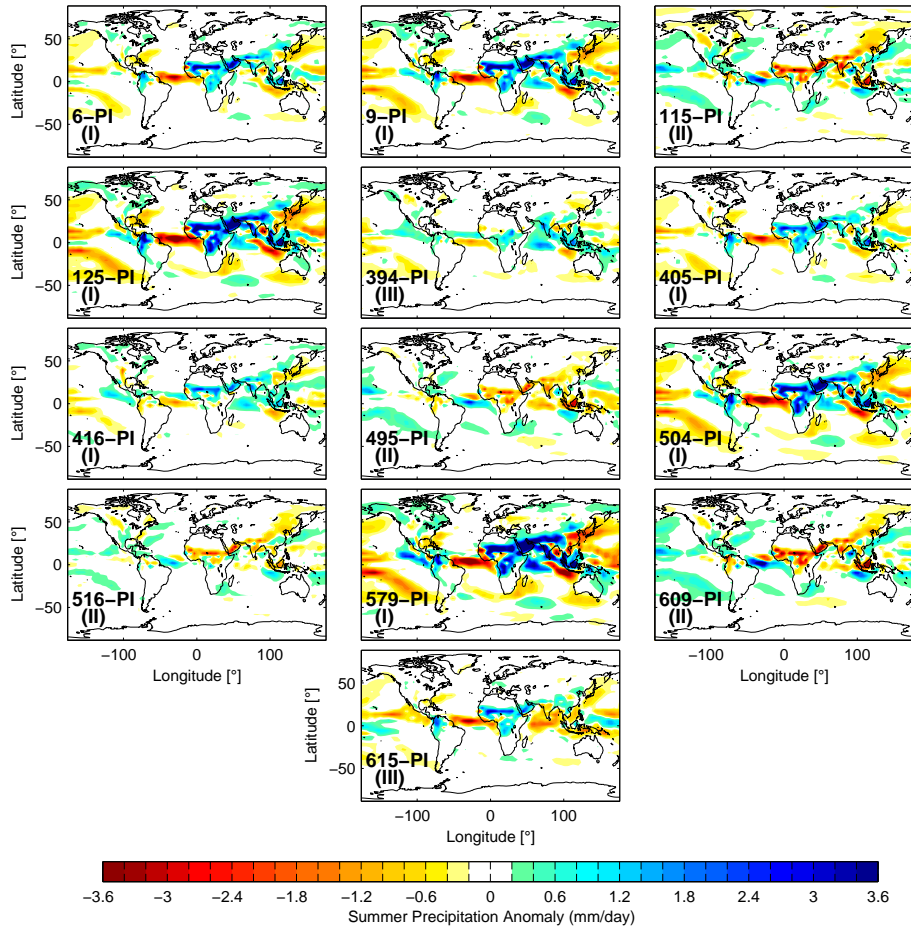


Figure 5. As in Fig. 3, but for boreal summer precipitation.

**Intra-interglacial climate variability from MIS 15 to the Holocene**

R. Rachmayani et al.

Title Page

Abstract Introduction

Conclusions References

Tables Figures

◀ ▶

◀ ▶

Back Close

Full Screen / Esc

Printer-friendly Version

Interactive Discussion



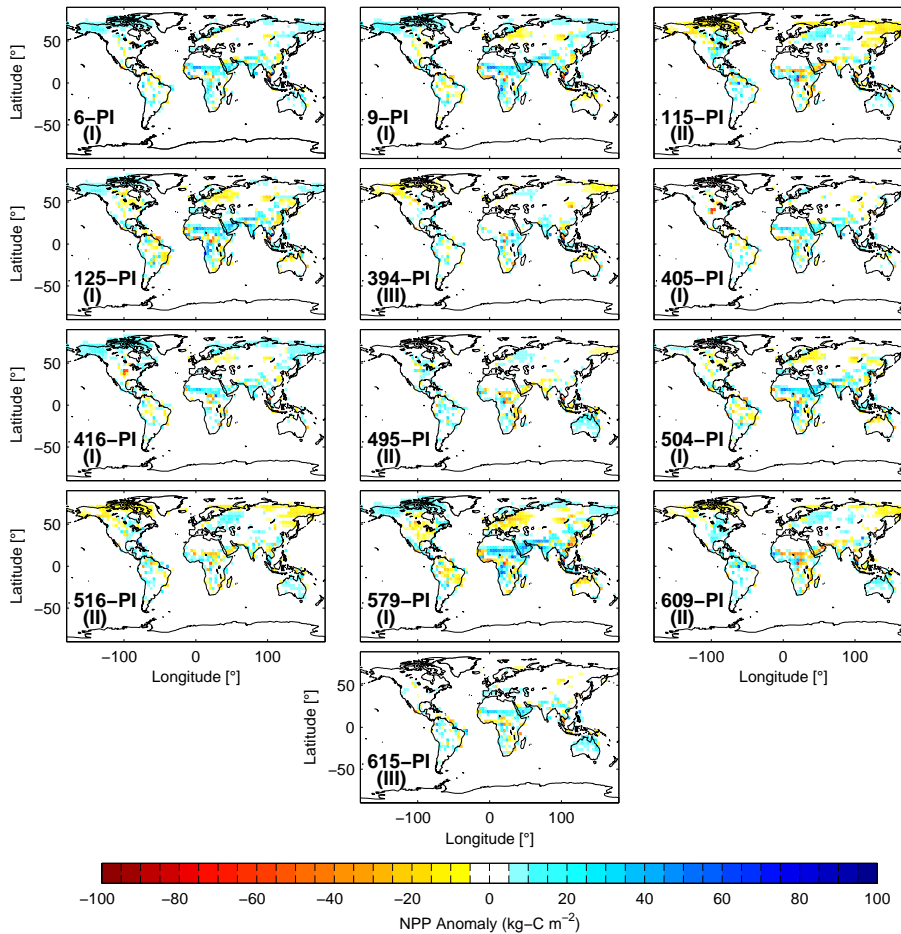


**Figure 6.** As in Fig. 3, but for annual net primary production.

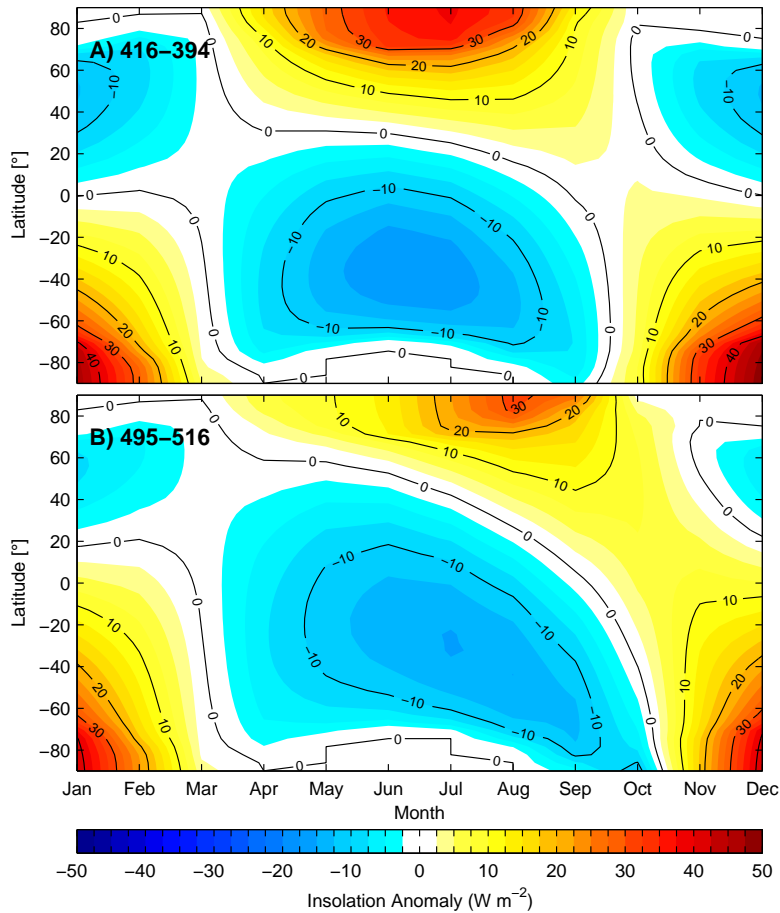


**Figure 7.** Differences in the seasonal and latitudinal distribution of insolation for **(a)** 416–394 kyr BP, **(b)** 495–516 kyr BP.

**Intra-interglacial  
climate variability  
from MIS 15 to the  
Holocene**

R. Rachmayani et al.

Title Page

Abstract

Introduction

Conclusions

References

Tables

Figures

◀

▶

◀

▶

Back

Close

Full Screen / Esc

Printer-friendly Version

Interactive Discussion



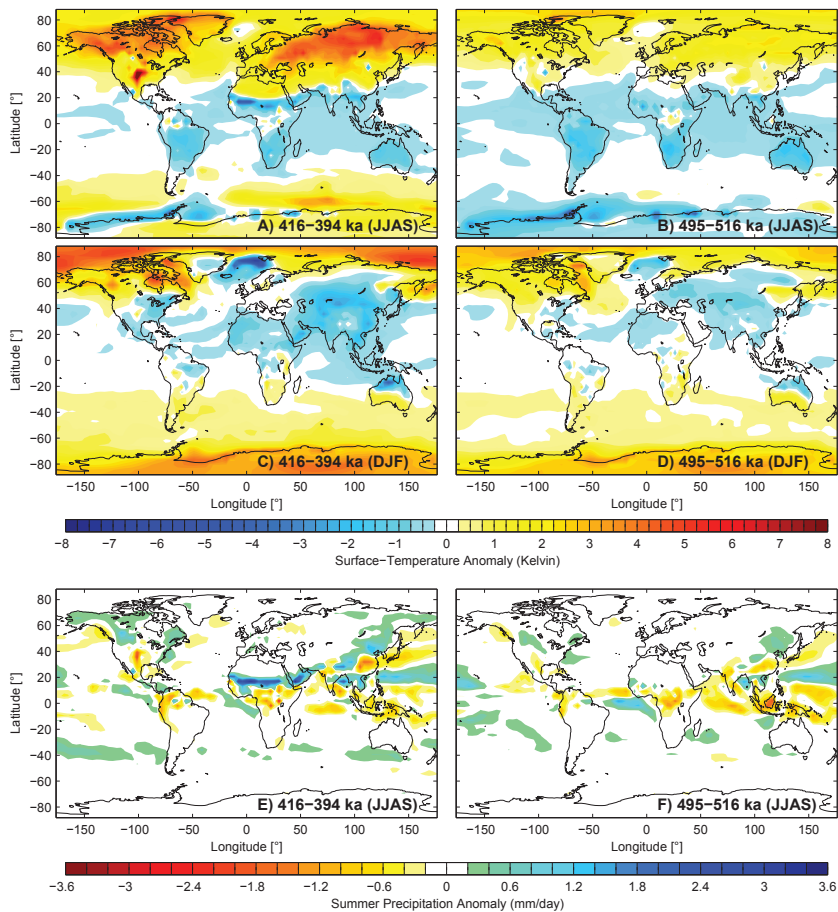


**Figure 8.** Differences in seasonal surface temperature (**a–d**) and boreal summer precipitation (**e**) and (**f**) for 416–394 kyrBP (left) and 495–516 kyrBP (right).

## Intra-interglacial climate variability from MIS 15 to the Holocene

R. Rachmayani et al.

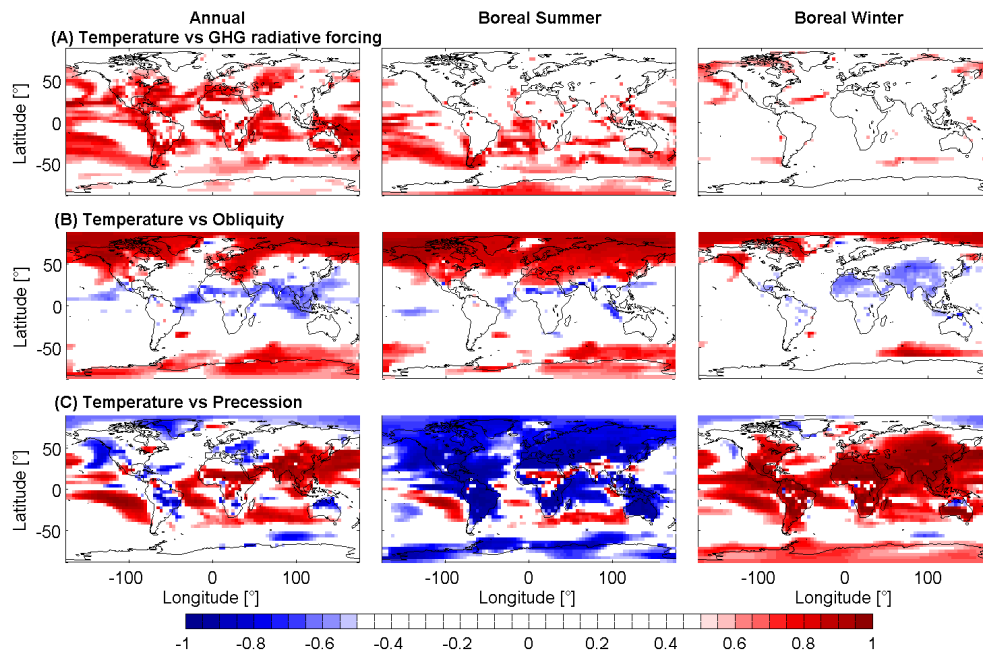


**Figure 9.** Linear correlation maps between surface temperature and GHG radiative forcing **(a)**, obliquity **(b)**, and climatic precession **(c)** as calculated from the entire set of experiments. Summer refers to JJAS, winter to DJF. Only significant values are shown according to a two-sided Student's  $t$  test at 95 % confidence level.

Title Page

Abstract

Introduction

Conclusions

References

Tables

Figures



Back

Close

Full Screen / Esc

Printer-friendly Version

Interactive Discussion



## Intra-interglacial climate variability from MIS 15 to the Holocene

R. Rachmayani et al.

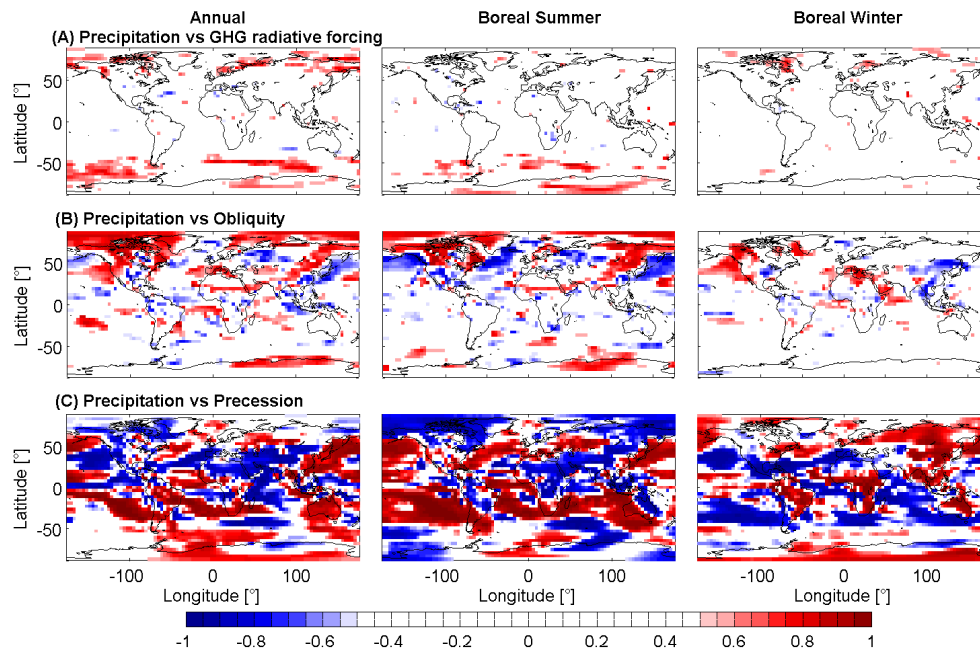


**Figure 10.** As in Fig. 9, but for precipitation.

Title Page

Abstract

Introduction

Conclusions

References

Tables

Figures



Back

Close

Full Screen / Esc

Printer-friendly Version

Interactive Discussion

